Utilizing Diruthenium Components for the Design of Cyanide-Linked Tri- and Tetranuclear Organometallic Complexes with Multistep One-Electron Redox Processes

Li-Yi Zhang,[†] Jing-Lin Chen,[†] Lin-Xi Shi,[†] and Zhong-Ning Chen*[,†,‡,§]

State Key Laboratory of Structural Chemistry, Fujian Institute of Research on the Structure of Matter, Chinese Academy of Sciences, Fuzhou, Fujian 350002, People's Republic of China, State Key Laboratory of Organometallic Chemistry, Shanghai Institute of Organic Chemistry, Chinese Academy of Sciences, Shanghai 200032, People's Republic of China, and State Key Laboratory of Coordination Chemistry, Nanjing University, Nanjing 210093, People's Republic of China

Received May 20, 2002

Reactions between the acetate-bridged diruthenium complex $Ru_2(O_2CCH_3)_4Cl$ and the cyanide-containing organometallic complex $Cp(dppe)FeCN$ or $Cp(PPh_3)_2RuCN$ brought about the isolation of the cyanide-linked tetranuclear complexes $[\{Cp(dppe)FeCN\}_2Ru_2(O_2CCH_3)_4](SbF_6)$ (**1**SbF_6) and $[\{Cp(PPh_3)_2RuCN\}_2Ru_2(O_2CCH_3)_4](SbF_6)$ (**2**SbF_6), while the similar reactions of the ap- or Fap-bridged (ap = 2-anilinopyridinate anion, Fap = 2-(2-fluoroanilino)-pyridinate anion) diruthenium complex $Ru_2(ap)_4Cl$ or $Ru_2(Fap)_4Cl$ with $Cp(dppe)FeCN$ or $Cp(PPh_3)_2RuCN$ gave the cyanide-linked trinuclear complexes $[Cp(dppe)FeCNRu_2(ap)_4](SbF_6)$ (**3**SbF_6), $[Cp(PPh_3)_2RuCNRu_2(ap)_4](SbF_6)$ (**4**SbF_6), $[Cp(dppe)FeCNRu_2(Fap)_4](SbF_6)$ (**5**SbF_6), and $[Cp(PPh_3)_2RuCNRu_2(Fap)_4](SbF_6)$ (**6**SbF_6). The structural analyses indicate that the steric effect is the predominant factor to govern the nuclearity of the cyanide-linked species. The steric hindrance derived from (4, 0) (for $Ru_2(ap)_4$) or (3, 1) (for $Ru_2(Fap)_4$) orientation in the diruthenium components is extremely unfavorable for the formation of the tetranuclear arrays $MCNRu_2(ap)_4NCM$ or $MCNRu_2(Fap)_4NCM$ (M = Fe or Ru) so as to afford the trinuclear assembly $MCNRu_2(ap)_4$ or $MCNRu_2(Fap)_4$ instead. The cyanide-linked complexes possess rich redox chemistry to afford two or more reversible redox processes. The complexes were characterized by elemental analysis, IR, UV−vis, ^{31}P NMR, and ES-MS spectroscopy, and cyclic voltammetry. The crystal structures of **2**SbF_6−**5**SbF_6 were determined by X-ray crystallography.

Introduction

Linearly assembled transition metal complexes that can exhibit multistep one-electron redox processes have attracted more and more attention due to the potential applications in electronics and optoelectronics.[1−7] Most of such molecular assemblies were designed by linkage of the redox-active mononuclear metal components such as $Cp^*(dppe)Fe$, $Cp(dppe)Fe$, $Cp(PPh_3)_2Ru$, $Cp^*(NO)(PPh_3)Re$, and *trans*-$Ru(dppm)_2$ through a linear organic ligand that can mediate electronic effects.[1] Utilizing the di-, tri-, or hexanuclear metal cluster components[8−17] that afford one or more one-electron redox couples for the design of the electronically delocalized molecules was involved only in a few cases due to the difficulty in controlling the linkage of the metal components through

* Corresponding author. Fax: +86-591-379-2346. E-mail: czn@ms.fjirsm.ac.cn.
† Fujian Institute of Research on the Structure of Matter.
‡ State Key Laboratory of Organometallic Chemistry.
§ State Key Laboratory of Coordination Chemistry.

(1) Paul, F.; Lapinte, C. *Coord. Chem. Rev.* **1998**, *178−180*, 1998.
(2) Cola, L. D.; Belser, P. *Coord. Chem. Rev.* **1998**, *177*, 301.
(3) Patoux, C.; Launay, J.-P.; Beley, M.; Chodorowski-Kimmes, S.; Collin, J.-P.; James, S.; Sauvage, J.-P. *J. Am. Chem. Soc.* **1998**, *120*, 3717.
(4) Berry, J. F.; Cotton, F. A.; Daniels, L. M.; Murillo, C. A. *J. Am. Chem. Soc.* **2002**, *124*, 3212.
(5) Cotton, F. A.; Lin, C.; Murillo, C. A. *Acc. Chem. Res.* **2001**, *34*, 759.
(6) Ziessel, R.; Hissler, M.; El-ghayoury, A.; Harriman, A. *Coord. Chem. Rev.* **1998**, *178−180*, 1251.
(7) (a) Constable, E. C.; Housecroft, C. E.; Schofield, E. R.; Encinas, S.; Armaroli, N.; Barigelletti, F.; Flamigni, L.; Figgemeier, E.; Vos, J. G. *Chem. Commun.* **1999**, 869. (b) Ortega, J. V.; Khin, K.; ven der Veer, W. E.; Ziller, J.; Hong, B. *Inorg. Chem.* 2**000**, *39*, 6038.
(8) (a) Miyasaka, H.; Campos-Fernández, C. S.; Clérac, R.; Dunbar, K. R. *Angew. Chem., Int. Ed.* **2000**, *39*, 3831. (b) Miyasaka, H.; Clérac, R.; Campos-Fernández, C. S.; Dunbar, K. R. *Inorg. Chem.* **2001**, *40*, 1663.
(9) (a) Abe, M.; Sasaki, Y.; Yamada, Y.; Tsukahara, K.; Yano, S.; Yamaguchi, T.; Tominaga, M.; Taniguchi, I.; Ito, T. *Inorg. Chem.* **1996**, *35*, 6724. (b) Ota, K.; Sasaki, H.; Matsui, T.; Hamaguchi, T.; Yamaguchi, T.; Ito, T.; Kido, H.; Kubiak, C. P. *Inorg. Chem.* **1999**, *38*, 4070.
(10) (a) Ren, T. *Organometallics* **2002**, *21*, 732. (b) Xu, G.; Ren, T. *Organometallics* **2001**, *20*, 2400.
(11) (a) Xue, W.-M.; Kühn, F. Z. *Eur. J. Inorg. Chem.* **2001**, 2041. (b) Xue, W.-M.; Kühn, F. Z.; Herdtweck, E.; Li, Q. *Eur. J. Inorg. Chem.* **2001**, 213.
(12) Hore, L.-A.; McAdam, C. J.; Kerr, J. L.; Duffy, N. W.; Robinson, B. H.; Simpson, J. *Organometallics* **2000**, *19*, 5039.
(13) Wong, K.-T.; Lehn, J. M.; Peng, S.-M.; Lee, G.-H. *Chem. Commun.* **2000**, 2259.
(14) Ren, T.; Zou, G.; Alvarez, J. C. *Chem. Commun.* **2000**, 1197.
(15) Bear, J. L.; Han, B.; Wu, Z.; Van Caemelbecke, E.; Kadish, K. M. *Inorg. Chem.* **2001**, *40*, 2275.
(16) Kuang, S.-M.; Fanwick, P. E.; Walton, R. A. *Inorg. Chem.* **2002**, *41*, 147.
(17) (a) Ito, T.; Hamaguchi, T.; Nagino, H.; Yamaguchi, T.; Kido, H.; Zavarine, I. S.; Richmond, T.; Washington, J.; Kubiak, C. P. *J. Am. Chem. Soc.* **1999**, *121*, 4625. (b) Yamaguchi, T.; Imai, N.; Ito, T.; Kubiak, C. P. *Bull. Chem. Soc. Jpn.* **2000**, *73*, 1205.

10.1021/om0203983 CCC: $22.00
Publication on Web 11/20/2002

an organic ligand. Furthermore, much fewer redox-active multinuclear cluster components[8−17] are available for the construction of the metal cluster-based multifunctional molecules compared with the mononuclear blocks that can be found numerously in the literature.[1]

The binuclear cluster complexes M_2L_4Cl (M = Ru, Rh) that can provide one- or multistep redox behavior are excellent precursors for the design of molecular assemblies with efficient electronic delocalization.[5,8,10,13−15] While most of the ligand-linked linear molecular assemblies consist of one type of metal components, those with two different types of the metal-containing building blocks have scarcely been touched.[11,16] Herein is described a new synthetic strategy for the design of cyanide-linked tri- and tetranuclear organometallic complexes with rich redox chemistry utilizing both the diruthenium and the mononuclear Fe- or Ru-containing organometallic components as the redox-active centers.

Experimental Section

Material and Preparation. All operations were performed in an atmosphere of dry argon by using Schlenk and vacuum techniques. Solvents were dried by standard procedures, distilled prior to use, and stored under argon. Solvents used in electrochemical measurements were of spectroscopic grade. All chemicals were commercially available (Acros, Fluka, and Aldrich Chemical Corp.) unless stated otherwise. The starting compounds $Ru_2(O_2CCH_3)_4Cl$,[18] $Ru_2(ap)_4Cl$ (ap = 2-anilinopyridinate anion),[19] $Ru_2(Fap)_4Cl$ (Fap = 2-(2-fluoroanilino)-pyridinate anion),[20] Cp(dppe)FeCN (dppe = 1,2-bis(diphenylphosphino)ethane), and $Cp(PPh_3)_2RuCN$ were prepared by the published procedures.[21]

Physical Measurements. Elemental analyses (C, H, N) were performed on a Perkin-Elmer model 240C automatic instrument. The electrospray mass spectra (ES-MS) were recorded on a Finngan LCQ mass spectrometer using dichloromethane−methanol as mobile phase. The UV−vis spectra in acetonitrile solutions were measured on a Perkin-Elmer Lambda 25 UV−vis spectrometer. The IR spectra were recorded on a Magna750 FT-IR spectrophotometer using KBr pellets. The $^{31}P\{H\}$ spectra were measured on a Bruker AM500 spectrometer with 85% H_3PO_4 as external standard. Magnetic measurements on powder samples were carried out with a CAHN-2000 Faraday-type magnetometer in the temperature range 80−300 K. The cyclic voltammogram was obtain by use of a Potentiostat/Galvanostat Model 263A in acetonitrile solutions containing 0.1 M $(Bu_4N)PF_6$ as supporting electrolyte at a scan rate of 100 mV s^{-1}. Platinum and glassy graphite were used as working and counter electrodes, respectively, and the potentials were measured against a Ag/AgCl reference electrode. The ferrocenium/ferrocene couple was observed at 0.585 V under the experimental conditions.

[{Cp(dppe)FeCN}$_2$Ru$_2$(O$_2$CCH$_3$)$_4$](SbF$_6$) (1SbF$_6$). To 30 mL of methanol−dichloromethane (1:2) was added Cp(dppe)-FeCN (0.20 mmol, 109.0 mg), $Ru_2(O_2CCH_3)_4Cl$ (0.10 mmol, 47.4 mg), and sodium hexafluoroantimonate (0.11 mmol, 28.5 mg) to produce a deep blue solution after stirring at room temperature for 2 h. Then the solvents were removed in vacuo to leave a dark blue residue, which was dissolved in 3 mL of dichloromethane. Layering hexane onto the solution gave blocked crystals. Yield: 73%. Anal. Calcd for $C_{72}H_{70}F_6Fe_2N_2O_8P_4Ru_2Sb{\cdot}CH_2Cl_2$: C, 47.40; H, 3.92; N, 1.51. Found: C, 47.28; H, 3.53; N, 1.41. ES-MS (*m*/*z*): 1529 ([{Cp(dppe)Fe}$_2$Ru$_2$(O$_2$CCH$_3$)$_4$]$^+$), 985 ([Cp(dppe)FeCNRu$_2$(O$_2$CCH$_3$)$_4$]$^+$), 546.1 (Cp(dppe)FeCN$^+$). IR (KBr, cm^{-1}): ν 2056s (CN), 1483m (ν_{as}(COO)), 1437s (ν_s(COO)), 658s (SbF_6^-). ^{31}P NMR ($CDCl_3$, ppm): 220.5 (s). UV−vis (λ_{max}/nm (ϵ, cm^{-1} M^{-1})): 269 (22100), 318 (12500), 630 (4470).

[{Cp(PPh$_3$)$_2$RuCN}$_2$Ru$_2$(O$_2$CCH$_3$)$_4$](SbF$_6$) (2SbF$_6$). The same synthetic procedure was employed as that for **1** except for the use of $Cp(PPh_3)_2RuCN$ instead of Cp(dppe)FeCN. Yield: 90%. Anal. Calcd for $C_{92}H_{82}F_6N_2O_8P_4Ru_4Sb{\cdot}CHCl_3$: C, 50.16; H, 3.76; N, 1.26. Found: C, 49.92; H, 3.43; N, 1.14. ES-MS (*m*/*z*): 1872 ({Cp(PPh$_3$)$_2$RuCN}$_2$Ru$_2$(O$_2$CCH$_3$)$_4$]$^+$), 1159 (Cp(PPh$_3$)$_2$RuCNRu$_2$(O$_2$CCH$_3$)$_4$]$^+$), 718 (Cp(PPh$_3$)$_2$RuCN$^+$). IR (KBr, cm^{-1}): ν 2063s (CN), 1481m (ν_{as}(COO)), 1435s (ν_s(COO)), 658s (SbF_6^-). ^{31}P NMR ($CDCl_3$, ppm): 217.2 (s) and 205.1 (s). UV−vis (λ_{max}/nm (ϵ, cm^{-1} M^{-1})): 270 (36100), 316 (13800), 511 (7250).

[Cp(dppe)FeCNRu$_2$(ap)$_4$](SbF$_6$) (3SbF$_6$). To a dichloromethane (10 mL) solution of Cp(dppe)FeCN (0.20 mmol, 109.0 mg) was added a dichloromethane (20 mL) solution of $Ru_2(ap)_4Cl$ (0.10 mmol, 91.4 mg), followed by the addition of a methane solution (5 mL) of sodium hexafluoroantimonate (0.11 mmol, 28.5 mg). After the solution was stirred at room temperature for 5 h, the solvents were evaporated in vacuo to leave a black-brown residue, which was redissolved in 3 mL of dichloromethane. Layering petroleum ether onto the solution gave prism crystals in one week. Yield: 81% (based on $Ru_2(ap)_4Cl$). Anal. Calcd for $C_{76}H_{65}F_6FeN_9P_2Ru_2Sb$: C, 54.99; H, 3.95; N, 7.59. Found: C, 55.47; H, 3.65; N, 7.29. ES-MS (*m*/*z*): 1425 ([Cp(dppe)FeCNRu$_2$(ap)$_4$]$^+$), 880 ($Ru_2(ap)_4^+$), 545 (Cp(dppe)-FeCN$^+$). IR (KBr, cm^{-1}): ν 2021s (CN), 1603s (ap), 658s (SbF_6^-). UV−vis (λ_{max}/nm (ϵ, cm^{-1} M^{-1})): 271 (55800), 329 (32900), 489 (6270), 785 (8690).

[Cp(PPh$_3$)$_2$RuCNRu$_2$(ap)$_4$](SbF$_6$) (4SbF$_6$). The same synthetic procedure was utilized as that for **3** except that Cp(dppe)FeCN was replaced by $Cp(PPh_3)_2RuCN$ to give dark brown crystals. Yield: 72%. Anal. Calcd for $C_{86}H_{71}F_6N_9P_2Ru_3Sb{\cdot}CH_2ClCH_2Cl$: C, 54.75; H, 3.92; N, 6.53. Found: C, 54.81; H, 3.68; N, 6.47. ES-MS (*m*/*z*): 1596 ([Cp(PPh$_3$)$_2$RuCNRu$_2$(ap)$_4$]$^+$), 880 ($Ru_2(ap)_4^+$), 717 (Cp(PPh$_3$)$_2$RuCN$^+$). IR (KBr, cm^{-1}): ν 2031s (CN), 1603s (ap), 658s (SbF_6^-). UV−vis (λ_{max}/nm (ϵ, cm^{-1} M^{-1})): 269 (41600), 328 (23800), 482 (5840), 789 (5990).

[Cp(dppe)FeCNRu$_2$(Fap)$_4$](SbF$_6$) (5SbF$_6$). To a dichloromethane (10 mL) solution of $Ru_2(Fap)_4Cl$ (0.10 mmol, 98.6 mg) was added first a dichloromethane solution (5 mL) containing Cp(dppe)FeCN (0.10 mmol, 54.5 mg), then a methanol (5 mL) solution of sodium hexafluoroantimonate (0.11 mmol. 28.5 mg). After the solution was stirred at room temperature for 6 h, the solvents were removed in vacuo to leave a dark green residue, which was redissolved in 3 mL of dichloromethane. Dark microcrystals were obtained by layering 10 mL of hexane onto the solution in a few days. Yield: 82%. Anal. Calcd for $C_{76}H_{61}F_{10}FeN_9P_2Ru_2Sb$: C, 52.70; H, 3.55; N, 7.28. Found: C, 52.70; H, 3.29; N, 7.16. ES-MS (*m*/*z*): 1497 ([Cp(dppe)-FeCNRu$_2$(Fap)$_4$]$^+$), 951 ($Ru_2(Fap)_4^+$), 546 (Cp(dppe)FeCN$^+$). IR (KBr, cm^{-1}): ν 2019s (CN), 1606s and 1489s (Fap), 658s (SbF_6^-). UV−vis (λ_{max}/nm (ϵ, cm^{-1} M^{-1})): 269 (42800), 329 (24300), 475 (4200), 767 (5020).

[Cp(PPh$_3$)$_2$RuCNRu$_2$(Fap)$_4$](SbF$_6$) (6SbF$_6$). The same synthetic procedure was employed as that for **5** except for the use of $Cp(PPh_3)_2RuCN$ instead of Cp(dppe)FeCN as the starting material. The product was isolated as brown-red crystals. Yield: 72%. Anal. Calcd for $C_{86}H_{67}F_{10}N_9P_2Ru_3Sb{\cdot}CH_2ClCH_2Cl$: C, 52.79; H, 3.57; N, 6.30. Found: C, 52.87; H, 3.29; N, 5.97. ES-MS (*m*/*z*): 1666 ([Cp(PPh$_3$)$_2$RuCNRu$_2$(Fap)$_4$]$^+$), 951 ($Ru_2(Fap)_4^+$), 718 (Cp(PPh$_3$)$_2$RuCN$^+$). IR (KBr, cm^{-1}): ν 2025s (CN), 1606s and 1489s (Fap), 658s (SbF_6^-). UV−vis (λ_{max}/nm (ϵ, cm^{-1} M^{-1})): 271 (53800), 332 (26200), 479 (4430), 757 (4850).

(18) Martin, D. S.; Newman, R. A.; Vlasnik, L. M. *Inorg. Chem.* **1980**, *19*, 3404.
(19) Chakravarty; Cotton, F. A.; Tocher, D. A. *Inrog. Chem.* **1985**, *24*, 172.
(20) Bear, J. L.; Wellhoff, J.; Royal, G.; Caemelbecke, E. V.; Eapen, S.; Kadish, K. M. *Inorg. Chem.* **2001**, *40*, 2282.
(21) Baird, G.; Davies, S. G. *J. Organomet. Chem.* **1984**, *262*, 215.

Table 1. Crystallographic Data for Compounds $2SbF_6 \cdot CHCl_3$, $3SbF_6 \cdot 2CH_2Cl_2$, $4SbF_6 \cdot CH_2ClCH_2Cl$, and $5SbF_6 \cdot 2CH_2ClCH_2Cl$

	$2SbF_6 \cdot CHCl_3$	$3SbF_6 \cdot CH_2Cl_2$	$4SbF_6 \cdot CH_2ClCH_2Cl$	$5SbF_6 \cdot 2CH_2ClCH_2Cl$
formula	$C_{93}H_{83}Cl_3F_6N_2O_8P_4Ru_4Sb$	$C_{77}H_{65}Cl_2F_6FeN_9P_2Ru_2Sb$	$C_{88}H_{75}Cl_2F_6N_9P_2Ru_3Sb$	$C_{80}H_{69}Cl_4F_{10}FeN_9P_2Ru_2Sb$
fw	1113.44	1742.96	1930.37	1929.92
color	dark red	black brown	brown	black green
cryst syst	monoclinic	triclinic	monoclinic	triclinic
space group	$P2_1/n$	$P\bar{1}$	$P2_1/n$	$P\bar{1}$
a, Å	12.5420(2)	13.8348(5)	13.7072(2)	12.4481(4)
b, Å	28.3700(5)	17.1541	18.5242(3)	18.0513(5)
c, Å	14.6127(3)	17.6275	34.91860(10)	18.0850(4)
α, deg		94.7770(10)		90.2940(10)
β, deg	101.88	107.022(2)	97.3760(10)	93.4780(10)
γ, deg		104.8850(10)		104.8520(10)
V, Å^3	5088.15(16)	3808.6(2)	8792.98(19)	3919.88
Z	2	2	4	2
D, g cm^{-3}	1.454	1.520	1.458	1.635
μ, cm^{-1}	10.45	11.02	9.67	11.52
$F(000)$	2222	1746	3868	1930
λ (Å, Mo Kα)	0.71073	0.71073	0.71073	0.71073
$2\theta_{max}$, deg	50.04	44.00	45.00	45.00
no. unique data	8820	9335	11501	10207
no obsd data for $I > 2\sigma(I)$	6626	5341	7627	6849
R_1[a]	0.0547	0.1215	0.0886	0.1040
wR_2[b]	0.1679	0.2668	0.2102	0.2048
goodness of fit	1.106	1.187	1.228	1.231
residual ρ, e Å^{-3}	1.468, −0.398	1.434, −0.725	1.347, −0.985	1.326, −0.832

X-ray Crystallography. Crystals of $2SbF_6 \cdot CHCl_3$ and $3SbF_6 \cdot CH_2Cl_2$ were grown by layering hexane onto the chloroform and dichloromethane solutions, respectively, whereas those of $4SbF_6 \cdot CH_2ClCH_2Cl$ and $5SbF_6 \cdot 2CH_2ClCH_2Cl$ were obtained from 1, 2-dichloroethane solutions by diffusion of petroleum ether. Crystal parameters and details for data collection and refinement are summarized in Table 1; full crystallographic data are provided in the Supporting Information.

Single crystals were coated with epoxy resin and mounted on a glass fiber or sealed in a capillary with mother liquor. Reflection data were collected at 293 K on a SIEMENS SMART CCD diffractometer by the ω scan technique at room temperature using graphite-monochromated Mo Kα ($\lambda = 0.71073$ Å) radiation. The data intensity was corrected for Lp factors, and the SADABS technique was applied for absorption corrections. The heavy atoms were located by direct methods, and the other non-hydrogen atoms were determined from the successive difference Fourier syntheses. The structures were refined on F^2 by the full-matrix least-squares method using the SHELXTL-97 program package.[22] The non-hydrogen atoms were refined anisotropically, whereas the hydrogen atoms were generated geometrically and refined with isotropic thermal parameters.

For $2SbF_6 \cdot CHCl_3$, the asymmetric unit contains half of the tetranuclear molecule, half an anion SbF_6^-, and half a solvate chloromethane. The occupancy factors of Sb, F, Cl, and C01 atoms are 0.5. For $3SbF_6 \cdot 2CH_2Cl_2$, the quality problem of the crystal led to a high R (0.1215) factor, but the refined structure was reliable and gave reasonable bonding data by fixing the C−Cl distances (1.760 ± 0.005 Å) of the solvate dichloromethane. The hydrogen atoms in dichloromethane were not added theoretically for the structural calculation. For $4SbF_6 \cdot CH_2ClCH_2Cl$ and $5SbF_6 \cdot 2CH_2ClCH_2Cl$, the structures were refined by fixing the C−C (1.525 ± 0.005 Å) and C−Cl (1.760 ± 0.005 Å) bond lengths of the solvate 1,2-dichloroethane.

Results and Discussion

Preparation and Characterization. While the combination between the diruthenium component $Ru_2(O_2CCH_3)_4^+$ and the cyanide-containing mononuclear block Cp(dppe)FeCN or $Cp(PPh_3)_2RuCN$ in 1:2 molar ratio gives the symmetrical tetranuclear assembly **1** or **2** (Scheme 1) in high yield, incorporation of the $Ru_2(ap)_4^+$ (or $Ru_2(Fap)_4^+$) and Cp(dppe)FeCN (or $Cp(PPh_3)_2RuCN$) afforded the trinuclear complexes **3**−**6** (Scheme 1) instead. It seems that the steric effect is a primary factor in governing the incorporation modes between the bi- and mononuclear components. The steric hindrance, resulting from (4, 0) or (3, 1) arrangements (Scheme 1) in the component $Ru_2(ap)_4^+$ or $Ru_2(Fap)_4^+$, allows the attachment of one component Cp(dppe)FeCN or $Cp(PPh_3)_2RuCN$ on one side of the diruthenium unit, but prohibits the linkage of another mononuclear component on the other side.

For **1** and **2**, the positive ion electrospray mass spectra showed three types of fragments including the tetranuclear complex ion $[\{Cp(dppe)FeCN\}_2Ru_2(O_2CCH_3)_4]^+$ (m/z 1529) or $[\{Cp(PPh_3)_2RuCN\}_2Ru_2(O_2CCH_3)_4]^+$ (m/z 1872), trinuclear ion $[Cp(dppe)FeCNRu_2(O_2CCH_3)_4]^+$ (m/z 985) or $[Cp(PPh_3)_2RuCNRu_2(O_2CCH_3)_4]^+$ (m/z 1158), and mononuclear component peak Cp(dppe)FeCN (m/z 545) or $Cp(PPh_3)_2RuCN$ (m/z 718), whereas the diruthenium component peak $Ru_2(O_2CCH_3)_4$ was unobserved. For **3**−**6**, three types of fragments appeared, including the complex ion peak, diruthenium component peak $Ru_2(ap)_4^+$ or $Ru_2(Fap)_4^+$, and the mononuclear component peak $Cp(dppe)FeCN^+$ or $Cp(PPh_3)_2RuCN^+$, coinciding perfectly with the anticipated ion fragments. The IR spectra of the cyanide-linked complexes **1**−**6** show a characteristic stretching vibration frequency of the cyanide. While the CN stretching bands in **1** (2056 cm^{-1}) and **2** (2063 cm^{-1}) exhibit a slight shift to lower frequencies, those in **3**−**6** move drastically to a much lower region (2019−2031 cm^{-1}) relative to the CN-containing parent compounds Cp(dppe)FeCN (2062 cm^{-1}) and $Cp(PPh_3)_2RuCN$ (2072 cm^{-1}). The ν(CN) shift to a lower frequency upon the formation of a cyanide-bridged moiety in **1**−**6** is assignable to the predominat-

(22) Sheldrick, G. M. *SHELXL-97*, Program for the Refinement of Crystal Structures; University of Göttingen: Germany, 1997.

Scheme 1

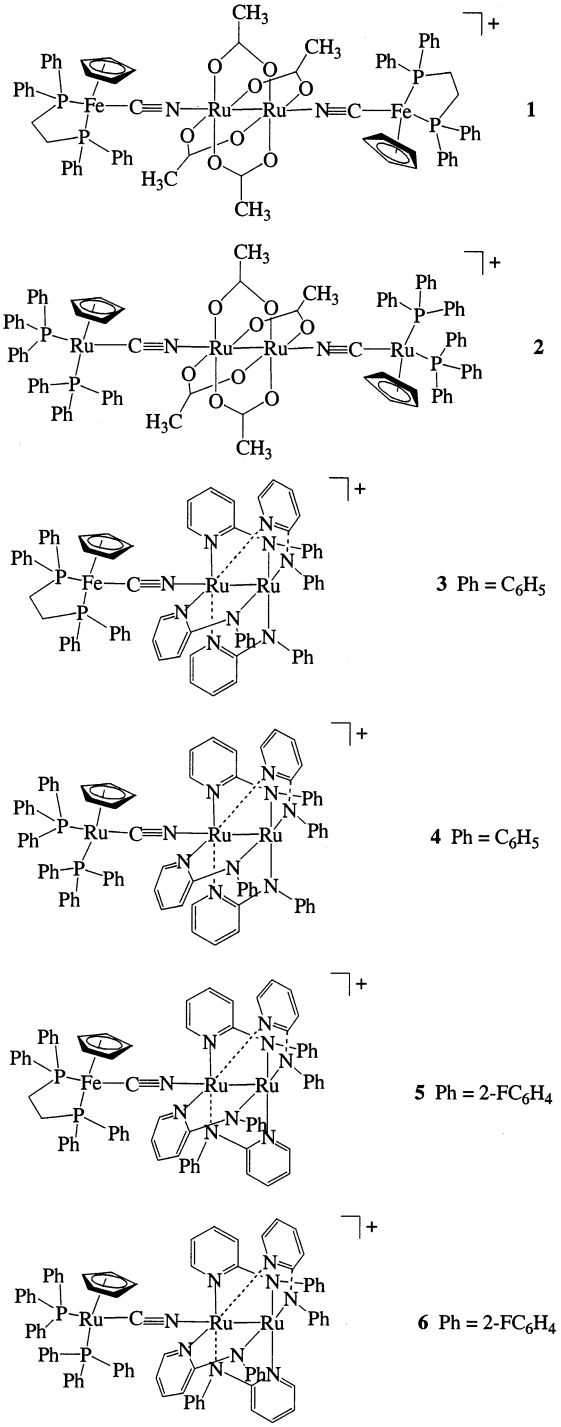

ing contribution from the π back-bonding donation.[23] The more prominent ν(CN) shift to a lower frequency for **3**−**6** compared with that for **1** and **2** can be elucidated readily since $Ru_2(ap)_2$ or $Ru_2(Fap)_2$ can provide a more efficient π back-bonding effect to the cyanide than the $Ru_2(O_2CCH_3)_4$. The magnetic moments for compounds **1**SbF_6, **5**SbF_6, and **6**SbF_6 at 300 K are 3.69, 4.22, and 3.93μ_B, respectively, corresponding to three unpaired electrons in the compounds as found for

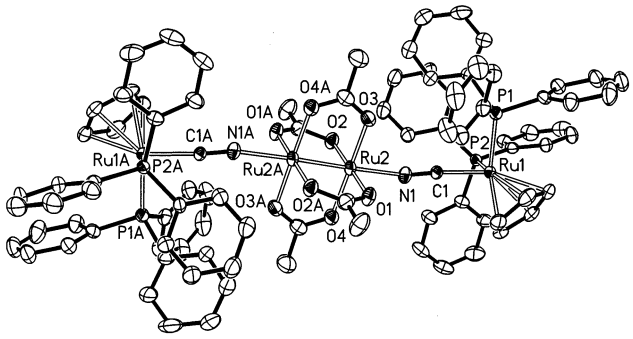

Figure 1. ORTEP drawing of $[\{Cp(PPh_3)_2RuCN\}_2Ru_2(CH_3COO)_4]^+$ (**2**) (30% thermal ellipsoids) with atom-labeling scheme.

the parent diruthenium compounds $Ru_2(O_2CR)_4Cl$ and $Ru_2(Fap)_4Cl$.[20,24] In the temperature range of 83−300 K, the magnetic behavior is also similar to that observed for the discrete cations $[Ru_2^{II,III}(O_2CR)_4]^+$,[24] in which the magnetic moments decrease with decreasing temperature due to the main contribution from zero-field splitting. Thus, the magnetic behavior of the diruthenium unit is unaffected by the attachment of the diamagnetic organometallic moiety Cp(dppe)FeCN or $Cp(PPh_3)_2$RuCN.

Crystal Structures. X-ray structural determinations of the complexes **2**SbF_6·$CHCl_3$, **3**SbF_6·CH_2Cl_2, **4**SbF_6·CH_2ClCH_2Cl, and **5**SbF_6·$2CH_2ClCH_2Cl$ have been performed; selected atomic distances and bond angles are presented in Table 2 for the purpose of comparison. Some common structural features are characteristic in the cyanide-linked tri- and tetranuclear complexes. First, the bridging arrays Fe−CN−Ru and Ru−CN−Ru are quasi-linear, in which the deviation from linearity in the N-bonded side is more pronounced than in the C-bonded side, except **4**, which exhibits a converse trend. Second, the C≡N distance is elongated about 0.06 Å relative to that (1.107(4) Å) in the parent compound $Cp(PPh_3)_2$RuCN, implying the C≡N bond is weakened upon formation of the bridging arrays Fe−CN−Ru and Ru−CN−Ru, which is also in accordance with the decrease of the ν(CN) observed in the IR spectra. For complex **2** (Figure 1), the tetranuclear ruthenium assembly is made up of one diruthenium component $Ru_2(O_2CCH_3)_4$ symmetrically connected by two mononuclear components CpFe(ddpe)CN through the cyanide bridges. The bridging array Ru1−C≡N−Ru2 deviates severely from linearity with Ru1−C≡N = 174.9(5)° and C≡N−Ru2 = 159.3(5)°, where the linearity of the C-bound end is obviously much better than that of the N end. The diruthenium unit $Ru_2(O_2CCH_3)_4$ remains the original pattern with the Ru−O distances in the range 2.027(5)−2.035(5) Å, close to those observed in the parent complex cation $Ru_2(O_2CCH_3)_4^+$.[18,25−27] The appreciably elongated Ru2−Ru2A distance (2.2959(10) Å) relative to those (2.248−2.287 Å) found in the parent

(23) (a) Coe, B. J.; Meyer, T. J.; White, P. S. *Inorg. Chem*. **1995**, *34*, 3600. (b) Richardson, G. N.; Brand, U.; Vahrenkamp, H. *Inorg. Chem*. **1999**, *38*, 3070. (c) Bignozzi, C. A.; Argazzi, R.; Schoonover, J. R.; Gordon, K. C.; Dyer, R. B. Scandola, F. *Inorg. Chem*. **1992**, *31*, 5260−5276.

(24) (a) Cukiernik, F. D.; Luneau, D.; Marchon, J.-C. Maidivi, P. *Inorg. Chem*. **1998**, *37*, 3698. (b) Barral, M. C.; Jiménez-Aparicio; Pérez-Quintanilla, D.; Priego, J. L.; Royer, E. C.; Torres, M. R.; Urbanos, F. A. *Inorg. Chem*. **2000**, *39*, 65.

(25) Bino, A.; Cotton, F. A.; Felthouse, T. R. *Inorg. Chem*. **1979**, *18*, 2599.

(26) Marsh, R. E.; Schomaker, V. *Inorg. Chem*. **1981**, *20*, 299.

(27) Drysdale, K. D.; Beck, E. J.; Cameron, T. S.; Robertson, K. N.; Aquino, M. A. S. *Inorg. Chim. Acta* **1997**, *256*, 243.

Table 2. Selected Bond Distances (Å) and Angles (deg) for Complexes 2−5

2		3		4		5	
Ru2−Ru2A	2.2957(10)	Ru1−Ru2	2.280(2)	Ru1−Ru2	2.2870(16)	Ru1−Ru2	2.2844(18)
Ru1−C1	1.966(6)	Fe1−C1	1.85(3)	Ru1−N21	2.043(11)	Fe1−C10	1.857(18)
Ru1−C71	2.238(6)	Fe1−P1	2.157(6)	Ru1−N41	2.037(11)	Fe1−P1	2.181(5)
Ru1−C72	2.236(6)	Fe1−P2	2.169(7)	Ru1−N61	2.008(11)	Fe1−P2	2.183(5)
Ru1−C73	2.222(7)	Ru1−N1	2.156(19)	Ru1−N81	2.031(12)	Ru1−N41	2.078(12)
Ru1−C74	2.227(7)	Ru1−N11	2.062(16)	Ru2−N11	2.104(11)	Ru1−N2	2.089(12)
Ru1−C75	2.253(7)	Ru1−N31	2.080(16)	Ru2−N31	2.107(13)	Ru1−N31	2. 105(11)
Ru1−P1	2.3053(16)	Ru1−N51	2.096(17)	Ru2−N51	2.099(11)	Ru1−N11	2.118(12)
Ru1−P2	2.3100(16)	Ru1−N71	2.0718(17)	Ru2−N71	2.096(11)	Ru−N10	2.172(13)
Ru2−N1	2.217(6)	Ru2−N21	1.995(16)	Ru2−N1	2.150(12)	Ru2−N3	2.039(12)
Ru2−O1	2.037(5)	Ru2−N41	2.004(16)	Ru3−C1	2.001(16)	Ru2−N4	2.040(2)
Ru2−O2	2.027(5)	Ru2−N61	1.985(15)	Ru3−P1	2.364(4)	Ru2−N1	2.042(12)
Ru2−O3	2.032(5)	Ru2−N81	2.003(15)	Ru3−P2	2.329(4)	Ru2−N21	2.057(13)
Ru2−O4	2.037(5)	N1−C1	1.17(2)	N1−C1	1.155(17)	N10−C10	1.166(18)
N1−C1	1.167(8)	N11−Ru1−N31	88.5(65)	N61−Ru1−N81	90.5(5)	N41−Ru1−N2	90.5(5)
O3−Ru2−O2	89.5(2)	N11−Ru1−N51	174.4(7)	N61−Ru1−N41	90.5(5)	N41−Ru1−N31	85.5(5)
O3−Ru2−O4	178.31(19)	N11−Ru1−N71	90.3(6)	N81−Ru1−N41	178.1(5)	N2−Ru1−N31	173.3(5)
O2−Ru2−O4	90.7(2)	N11−Ru1−N1	92.8(7)	N61−Ru1−N21	179.7(5)	N41−Ru1−N11	174.1(5)
O3−Ru2−O1	90.3(2)	N31−Ru1−N51	89.9(6)	N81−Ru1−N21	89.3(5)	N2−Ru1−N11	89.5(5)
O2−Ru2−O1	178.39(18)	N31−Ru1−N1	91.8(7)	N41−Ru1−N21	89.8(5)	N31−Ru1−N11	94.0(4)
O4−Ru2−O1	89.5(2)	N51−Ru1−N1	92.6(6)	N61−Ru1−Ru2	90.4(3)	N41−Ru1−N10	94.4(5)
O3−Ru2−N1	88.8(2)	N71−Ru1−N31	176.1(7)	N81−Ru1−Ru2	89.6(3)	N2−Ru1−N10	95.7(5)
O2−Ru2−N1	92.0(2)	N71−Ru1−N51	91.0(6)	N41−Ru1−Ru2	88.8(4)	N31−Ru1−N10	89.9(5)
O4−Ru2−N1	92.9(2)	N71−Ru1−N1	92.0(7)	N21−Ru1−Ru2	89.7(3)	N11−Ru1−N10	91.5(5)
O1−Ru2−N1	89.55(19)	N11−Ru1−Ru2	87.3(5)	N71−Ru2−N51	91.7(4)	N41−Ru1−Ru2	87.7(3)
O1−Ru2−Ru2A	89.02(13)	N71−Ru1−Ru2	86.8(5)	N71−Ru2−N11	91.0(4)	N2−Ru1−Ru2	89.0(3)
O2−Ru2−Ru2A	89.38(13)	N31−Ru1−Ru2	89.4(5)	N51−Ru2−N11	173.2(4)	N31−Ru1−Ru2	85.5(3)
O3−Ru2−Ru2A	88.63(14)	N51−Ru1−Ru2	87.3(5)	N71−Ru2−N31	175.2(5)	N11−Ru1−Ru2	86.4(4)
O4−Ru2−Ru2A	89.69(13)	N1−Ru1−Ru2	178.8(5)	N51−Ru2−N31	88.7(4)	N10−Ru1−Ru2	174.8(3)
N1−Ru2−Ru2A	177.04(15)	N61−Ru2−N21	179.6(7)	N11−Ru2−N31	88.1(5)	N3−Ru2−N4	90.5(5)
N1−C1−Ru1	174.9(5)	N61−Ru2−N81	89.1(6)	N71−Ru2−N1	90.8(4)	N3−Ru2−N1	90.0(5)
C1−N1−Ru2	159.3(5)	N21−Ru2−N81	90.7(6)	N51−Ru2−N1	94.5(4)	N4−Ru2−N1	179.4(6)
		N61−Ru2−N41	89.96)	N11−Ru2−N1	91.7(4)	N3−Ru2−N21	177.6(5)
		N21−Ru2−N41	90.3(6)	N31−Ru2−N1	93.9(5)	N4−Ru2−N21	89.5(5)
		N81−Ru2−N41	179.0(6)	N71−Ru2−Ru1	87.2(3)	N1−Ru2−N21	90.0(5)
		N61−Ru2−Ru1	90.8(5)	N51−Ru2−Ru1	87.3(3)	N3−Ru2−Ru1	89.5(3)
		N21−Ru2−Ru1	89.6(5)	N11−Ru2−Ru1	86.6(3)	N4−Ru2−Ru1	89.6(3)
		N81−Ru2−Ru1	90.2(4)	N31−Ru2−Ru1	88.1(3)	N1−Ru2−Ru1	90.6(4)
		N41−Ru2−Ru1	89.8(5)	N1−Ru2−Ru1	177.4(3)	N21−Ru2−Ru1	88.1(3)
		N1−C1−Fe1	178.4(18)	N1−C1−Ru3	169.2(12)	N10−C10−Fe1	172.8(13)
		C1−N1−Ru1	170.4(16)	C1−N1−Ru2	173.1(11)	C10−N10−Ru1	166.1(13)

diruthenium complexes[18,25−27] can be attributed to the electron-withdrawing character of the CN-containing organometallic component CpFe(ddpe)CN, which draws the electronic density away from the Ru_2 moiety and hence weakens the Ru−Ru bond. The Ru1···Ru2 separation through the bridging cyanide is 5.262 Å, whereas the distance of Ru1···Ru1A reaches as long as 12.756 Å along the molecular rod.

The heterotrinuclear complex **3** (Figure 2) is derived from the diruthenium component $Ru_2(ap)_4$ associated with the mononuclear component Cp(dppe)FeCN through

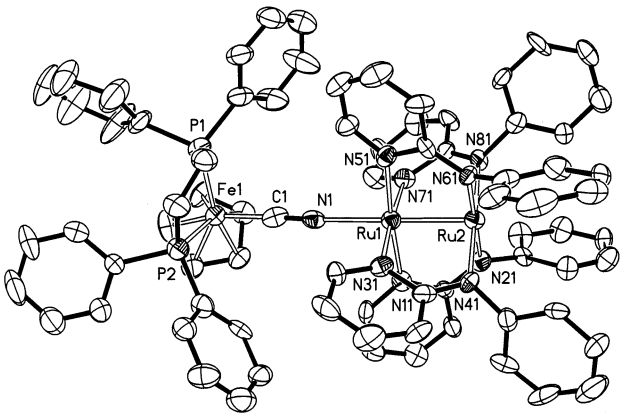

Figure 2. ORTEP drawing of $[Cp(dppe)FeCNRu_2(ap)_4]^+$ (**3**) (30% thermal ellipsoids) with atom-labeling scheme.

cyanide linkage. As observed in the parent compound $Ru_2(ap)_4Cl$,[19] the diruthenium component $Ru_2(ap)_4$ adopts a (4, 0) conformation, where one ruthenium atom (Ru1) is coordinated by four pyridine nitrogen atoms and one axial cyanide nitrogen atom (N1), while the other ruthenium center (Ru2) is coordinated by four amine nitrogen atoms. Such an orientation for the four ap favors the attachment of a CN-containing component along one side but brings about a severe steric effect on the other side. Thus, the isolation of a heterotri- instead of a heterotetranuclear assembly by the incorporation of the diruthenium component $Ru_2(ap)_4$ and Cp(dppe)FeCN is elucidated reasonably. The Ru1−Ru2 (2.278(2) Å) distance in the $Ru_2(ap)_4$ moiety is almost the same as that (2.275(3) Å) in the parent compound $Ru_2(ap)_4Cl$,[19] whereas the Ru−N (1.983(14)−2.007(14) Å) distances become slightly shorter compared with those (2.023(12)−2.105(11) Å) in the parent comound.[19] The bridging array Ru−N≡C−Fe is quasi-linear, with the linearity of the C-bound end (N1−C1−Fe1 = 178.1(17)°) being better than that of the N-bound end (C1−N1−Ru1 = 170.0(16)°). The Fe1···Ru1 separation through the cyanide is 5.161 Å, and the Fe1···Ru2 distance is 7.427 Å.

In the complex cation $[Cp(PPh_3)_2RuCNRu_2(ap)_4]^+$ (**4**), the diruthenium moiety $Ru_2(ap)_4$ retains the same (4, 0) conformation as mentioned above for **3**. The Ru1−Ru2 (2.2870(16) Å) distance is close to that in **3**

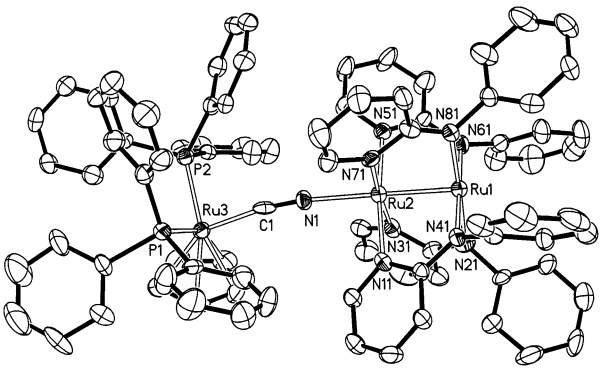

Figure 3. ORTEP drawing of $[Cp(PPh_3)_2RuCNRu_2(ap)_4]^+$ (**4**) (30% thermal ellipsoids) with atom-labeling scheme.

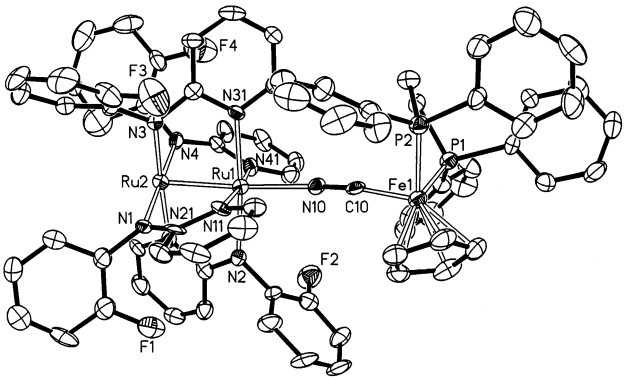

Figure 4. ORTEP drawing of $[Cp(dppe)FeCNRu_2(Fap)_4]^+$ (**5**) (30% thermal ellipsoids) with atom-labeling scheme.

(2.278(2) Å) as well as in the parent complex $Ru_2(ap)_4Cl$ (2.275(3) Å).[19] For the bridging array Ru−C≡N−Ru, the linearity of the C-bonded side (Ru3−C1−N1 = 169.2(12)°) is a little worse than that of the N-bonded side (Ru−N−C = 173.1(11)°), in contrast with that observed in **2** and **3**. The Ru2···Ru3 separation through the cyanide is 5.264 Å, and the Ru1···Ru3 distance is 7.537 Å, both of which are slightly longer compared with those in **3**.

In the complex **5** (Figure 4), the diruethnium moiety $Ru_2(Fap)_4$ exhibits a (3, 1) pattern as in the parent compound $Ru_2(Fap)_4Cl$,[20] giving rise to the formation of a cyanide-linked tri- instead of tetranuclear assembly because of the remarkable steric effects. The Ru1−Ru2 (2.2844(18) Å) and Ru−N (2.039(12)−2.118(12) Å) distances almost remain unchanged relative to those in the parent compound $Ru_2(Fap)_4Cl$.[20] The average Ru1−N distance (2.098 Å) is 0.053 Å longer than the average Ru2−N (2.045 Å) distance due to the lack of an axial ligand on the Ru2 atom, as observed in $Ru_2(Fap)_4Cl$.[20] For the CN bridging array, the C-bound side (172.8(13)°) is more close to linearity than the N-bound side (166.1(13)°). The Ru1···Fe1 separation through the cyanide bridge is 5.141 Å, whereas the Ru2···Fe1 distance through the molecular rod is 7.394 Å.

Electrochemistry. The electrochemical data of compounds **1**SbF_6−**6**SbF_6 are shown in Table 3. The heterotetranuclear complexes **1** and **2** display two quasi-reversible redox processes. The cathodic couple ($E_{1/2}$(red) = −0.335 V for **1** and −0.292 V for **2**) belongs to the reduction of the diruthenium component $Ru_2^{II,III}(O_2CCH_3)_4$, whereas the anodic couple ($E_{1/2}$(ox1) = +0.658 V for **1** and +0.986 for **2**) can be assigned to the

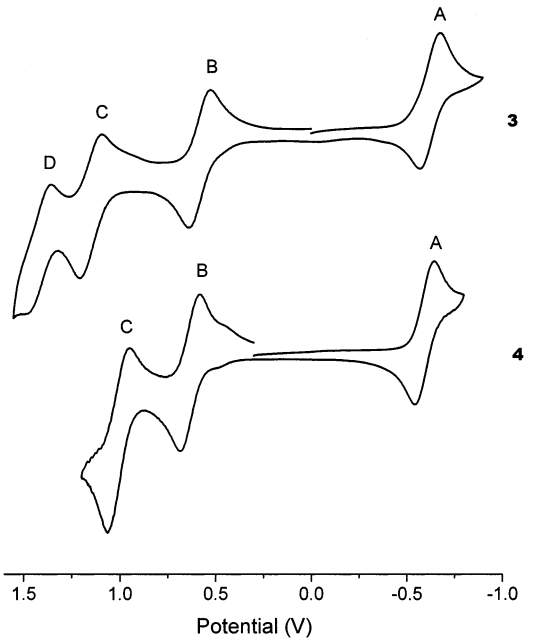

Figure 5. Cyclic voltammograms of complexes **3** and **4** recorded in 0.10 M dichloromethane solution of Bu_4NPF_6 at a scan rate of 0.10 V/s.

oxidation process of the organometallic moiety Cp(dppe)-Fe or $Cp(PPh_3)_2Ru$ on the basis of the $E_{1/2}$ for the parent compounds Cp(dppe)FeCN ($E_{1/2}$ = +0.480 V) and $Cp(PPh_3)_2RuCN$ ($E_{1/2}$ = +0.795 V). The anodic couple results from a two-electron oxidation process because the electrical current strength for the anodic couple is almost doubled relative to that for the cathodic couple, which is due to a one-electron redox process. The rather long distance (>12.7 Å for **1**) between the organometalllic units at each end of the quasi-linear teranuclear molecule may elucidate the lack of an obvious electronic interaction, confirming further the fact that the dinuclear component $M_2(O_2CCH_3)_4$ is always unfavorable to transmit an efficient electronic communication between two axially bonded redox-active centers.[11] Thus, the redox processes on **1** can be summarized as follows:

$$[(Fe^{III}CN)_2Ru^{II}Ru^{III}]^{3+} \underset{-2e}{\overset{+2e}{\rightleftharpoons}} [(Fe^{II}CN)_2Ru^{II}Ru^{III}]^{+} \underset{-e}{\overset{+e}{\rightleftharpoons}} [(Fe^{II}CN)_2Ru^{II}Ru^{II}]^{0}$$

The rich redox characteristics of the $Ru_2(ap)_4$-containing complexes **3** and **4** are revealed by the cyclic voltammograms shown in Figure 5. While **3** shows four quasi-reversible couples at $E_{1/2}$ = −0.623, +0.587, +1.149, and 1.390 V, **4** undergoes three quasi-reversible one-electron redox processes at −0.594, +0.633, and 1.006 V. For **4**, the reversible waves disappear when the range of potential sweep is extended beyond 1.2 V, revealing an oxidative degradation in the high potential range. In reference to the redox potentials of the parent compounds $Ru_2(ap)_4Cl$ ($E_{1/2}$ = −0.790 and 0.486 V),[28] Cp(dppe)FeCN ($E_{1/2}$ = +0.480 V), and $Cp(PPh_3)_2RuCN$ (($E_{1/2}$ = +0.795 V), the $E_{1/2}$(red), $E_{1/2}$(ox1), and $E_{1/2}$(ox3) can be ascribed to the $Ru_2^{II,III}(ap)_4$-centered redox

(28) Zou, G.; Alvarez, J. C.; Ren, T. *J. Organomet. Chem.* **2000**, *596*, 152.

Table 3. Electrochemical Data for Complexes 1−6

	1	2	3	4	5	6
$E_{1/2}$(red)/(ΔE_P)	−0.335(0.106)	−0.292(0.140)	−0.623(0.106)	−0.594(0.100)	−0.510(0.100)	−0.426(0.180)
$E_{1/2}$(ox1)/(ΔE_P)	+0.658 (0.152)	+0.986 (0.156)	+0.578(0.108)	+0.633(0.102)	+0.647(0.098)	+0.680(0.082)
$E_{1/2}$(ox2)/(ΔE_P)			+1.149(0.110)	+1.006(0.116)	+0.988(0.148)	
$E_{1/2}$(ox3)/(ΔE_P)			+1.390(0.147)		+1.600(0.114)	

processes, whereas $E_{1/2}$(ox2) is assignable to the oxidation of the organometallic moiety Cp(dppe)Fe or Cp(PPh$_3$)$_2$Ru. It is obvious that the positive potential shifts of the $Ru_2^{II,III}(ap)_4$-centered and organometallic-based redox potentials relative to the parent compounds reflect the electronic effect upon the formation of the cyanide-linked arrays. The observed redox processes of **3** and **4** can thus be expressed as a member of a five-component electron transfer series according to the scheme below:

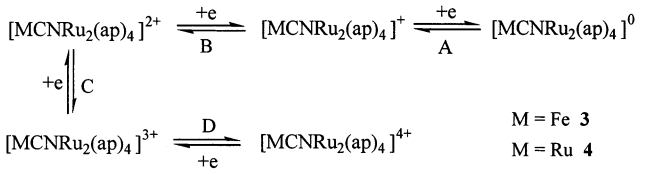

The electrochemical behavior of the $Ru_2(Fap)_4$-containing complexes **5** and **6** is similar to that of **3** and **4**. As listed in Table 3, the Cp(dppe)Fe-containing complex **5** exhibits a single quasi-reversible one-electron reduction and three reversible one-electron oxidations, while the Cp(PPh$_3$)$_2$Ru-containing complex **6** is characterized by a single quasi-reversible reduction and one single reversible oxidation. The reversible oxidation waves disappear once the potential sweep is beyond 1.0 V because of the oxidative decomposition at a high potential scale.

Conclusions

The present study demonstrates a new synthetic strategy for the design of cyanide-linked tri- and tetranuclear complexes with a linear metal assembly utilizing the redox-active mono- and binuclear metal components as building blocks, where the mononuclear organometallic unit possesses potential bridging character, whereas the diruthenium component offers substitutable coordination sites. The nuclearity of the linear assembled complexes is determined by the steric effect resulting from different orientations of the bridging ligands in the diruthenium components. The cyanide-linked complexes afford a rich electrochemical behavior and exhibit multistep reversible one-electron redox processes.

Acknowledgment. We are grateful for the financial support from NSF of China (No. 20171044) and the project for "hundred talents" from the Chinese Academy of Sciences.

Supporting Information Available: Tables of all atomic positional and equivalent isotropic displacement parameters, anisotropic displacement parameters, and all bond distances and bond angles of compounds **2**$SbF_6 \cdot CHCl_3$, **3**$SbF_6 \cdot CH_2Cl_2$, **4**$SbF_6 \cdot CH_2ClCH_2Cl$, and **5**$SbF_6 \cdot 2CH_2ClCH_2Cl$. This material is available free of charge via the Internet at http://pubs.acs.org.

OM0203983